Nonlinear dynamics of shape memory alloys actuated bistable beams

IOP Publishing Smart Materials and Structures
Smart Mater. Struct. **28** (2019) 055009 (14pp) https://doi.org/10.1088/1361-665X/ab0325

Nonlinear dynamics of shape memory alloys actuated bistable beams

Jiaying Zhang[1,2], Zhangming Wu[3], Chen Zhang[4], Lin Hao[4], Rui Nie[4] and Jinhao Qiu[4]

[1] College of Engineering, Swansea University, Swansea, SA1 8EN, United Kingdom
[2] Department of Mechanical and Aerospace Engineering, University of Strathclyde, Glasgow, G1 1XJ, United Kingdom
[3] Cardiff School of Engineering, Cardiff University, Cardiff, CF24 3AA, United Kingdom
[4] State Key Laboratory of Mechanics and Control of Mechanical Structures, Nanjing University of Aeronautics and Astronautics, Nanjing 210016, People's Republic of China

E-mail: Jiaying.Zhang@Swansea.ac.uk

Received 9 October 2018, revised 9 January 2019
Accepted for publication 30 January 2019
Published 5 April 2019

Abstract

The phenomenon of bi-stable behaviour has been widely used in the structural design, as it can provide large deformation by switching between two stable equilibrium positions. This paper aims to investigate the intrinsic nonlinear dynamic characteristics of an actively controlled bistable beam using a simplified spring-mass model. The dynamic model for an active (heated) SMA wire driven bistable beam is established based on a polynomial constitutive equation to describe the thermomechanical behaviour of the shape memory alloy. The actively controlled bistable beams are designed, fabricated and experimentally tested to achieve the morphing behaviour snapping-through form one position to another. The results obtained from the experimental testing and the theoretical simulation are compared to validate the proposed model. Dynamic behaviour of the proposed SMA wires actuated bistable beam under varying external excitation is investigated to show the influence of the thermomechanical loadings. Analysis of the experimental data and simulation results shows that the SMA wires actuated bistable structure can be well-performed for the bistable switching. It also approved that the different behaviours of the system, including periodic responses, complex responses and chaos can be accurately predicted using the proposed simplified model.

Keywords: bistable structures, shape memory alloys, nonlinear dynamics

(Some figures may appear in colour only in the online journal)

1. Introduction

There are many physical examples in the natural world exhibit multiple stable characteristics, such as the Venus flytrap, plant leafs and seedpods [1–3]. In recent years, this multi-stable structural phenomenon has attracted considerable research interests in developing advanced structures with smart functionality, in particular for the engineering applications in energy harvesting and morphing aircrafts [4–12]. The multi-stable structures with the capacity of shape-changing can receive many engineering applications in the Aerospace, Energy and Marine industrial sectors, where always demand the structures can transit between two or more stable positions for achieving benign performance with respect to the varying surrounding circumstances. Moreover, another outstanding feature of multi-stable structures is that neither any power nor any locking mechanisms are required to enable them to remain in stable positions.

A bistable beam is one of the simplest forms that are widely used to construct multistable mechanical structures. Moreover, the nonlinearity of its structural and dynamic behaviour can be exploited for broad engineering applications. Pontecorvo *et al* [9] applied a series of bistable arches to design a multistable cellular honeycomb-like structure, which is able to undergo large deformations for the chord extension morphing application of a helicopter rotor. Both

numerical simulation and experimental setup have been carried out in their work [9] to demonstrate the bistable beams in morphing applications. A centrifugally actuated von Mises truss has also been designed to implement the passive chord morphing mechanism for helicopter rotor blades in Moser *et al*'s work [10]. Moreover, the multistable morphing structures provide promising design solutions for micro-actuators and optical switching in MEMS devices. Liu *et al* [13] designed a micro-actuator device with two rows of bistable micro-actuators, which are formed by antagonistic pre-shaped double beams. Brenner *et al* [14] proposed an optimal design of this type bistable switch that possesses a better force–displacement characteristic. The multistable morphing structures have also attracted considerable research interests and broad applications in energy harvesting and energy dissipation [4, 5, 15–17]. For example, a piezoelectric energy harvester was designed by utilising the snap-through motions from the bistable behaviour to produce electrical power under low-frequency excitations [5, 15]. Many other research efforts that take advantages of the multistable structures have been made for vibrations absorption [16, 17]. A single degree-of-freedom mass-spring is designed as a bistable system, which is used to study the problem of forced oscillations absorption [16]. A more practical model formed by von-Mises truss (VMT) is introduced to analyse the dissipation properties and examine the energy absorption of a bistable system [17].

Moreover, different scales devices and structures have been investigated to demonstrate the practical applications of utilising the nonlinear dynamical characteristics of a bistable system. Sulfridge *et al* presented a nonlinear dynamics analysis for a bistable MEMS—a buckled micromechanical beam that was switched from one stable state to the other by the radiation pressure [18]. Their nonlinear dynamic model predicts that the buckled beam can be toggled by a transverse force, which is slightly higher than the toggling threshold force. This work sheds lights on the rich dynamics of micromechanical bistable systems for the application in switching. Krylov *et al* investigated another pre-buckled electrostatically actuated beam for the feasibility of two-directional switching by fringing electrostatic fields [19]. The general results presented in their work shed lights on the intrinsic nonlinearities of micro-devices on the structural stability, which can be exploited by designers in MEMS/NEMS based applications, e.g. electromechanical switches, biosensors etc. Aimmanee *et al* studied the snap-through buckling behaviour of a buckled beam bonded with segmented piezoelectric actuators using a mathematical model, and validated the theoretical predictions with experiments [20]. Different with these static switching strategies, Casals-Terré *et al* proposed a dynamic snapping strategy that can switch between states of a bistable mechanism utilising mechanical resonance phenomenon [21]. They demonstrated that if a bistable structure is driven into a resonance near one of its stable states, a sufficiently large amplitude of vibration may be achieved to switch between its stable states [21].

In recent years, smart materials were always applied to implement the actuation mechanism for the transition capability of multi-stable structures. The internal properties of these smart materials can be changed under external stimuli, such as stress, temperature, electric or magnetic fields. Therefore, they are ideally used for implementing the smart functionalities of multi-stable structures [22]. Shape memory alloy (SMA) which is a typical smart material possesses the properties of shape memory effect and pseudoelasticity [23]. As such, the SMA wire had been widely used to control structural behaviour [24, 25], for example the flexible biomimetic fin [26] and tentacles [27] in the bionic applications. The dynamic characteristics of SMA based structural systems have been studied to possess specific properties [28, 29], for example, Boeing has developed an active serrated aerodynamic device with SMA, which has been proven to be very effective in reducing noise during take-off [30, 31]. The dynamic characteristics of a planar bending actuator embedded with a SMA have been investigated to accurately predict the deflection process [32]. The planar bending actuator is constructed by an elastic substrate and an embedded SMA wire. This type of planar actuator is able to generate relatively large stress and strain through stimulating the SMA wires [32]. Therefore, SMA actuated structures have been widely employed in the temperature-dependent applications. For example, a SMA-pendulum system and an adaptive origami-stent system are proposed to present temperature-dependent behaviour of the SMA and the possibility of thermal control of the system [33]. Temperature variations can be employed to change either the position (static) or the response (dynamic) of a SMA based system in a variety of ways. The creation or suppression of chaos and the orbit changes can be analysed by actuating SMA [33, 34].

In this paper, the near-equiatomic NiTi alloy wires are utilised to drive a bistable beam, actively. A simplified analytical model is then developed to study the nonlinear dynamics of SMA wires actuated bistable beams. The capability of applying SMA wires to influence the dynamical characteristics of the bistable system is, for the first time, investigated. It is worth to mention that the response of SMA wire actuators is too slow to be applied for the vibration control, but the thermomechanical property of SMA wires can be utilised to affect the dynamic characteristics of the system. For example, a bi-stable VMT integrated with SMA wires to provide the actuation force for the transition of the VMT between two stable equilibrium conditions [35]. SMA wires have been designed to column joint with a beam towards the stiffness and energy dissipative ability [36]. Moreover, SMA wires are designed as a suspension to support a rotor-bearing test rig to reduce the vibration level of rotating systems [37]. In addition, SMA wires have been widely used in the construction of morphing structures, for example, the SMA wires were designed to be attached to the hexa-pivotal joint to produce a shape morphing hinged truss structures [38]. In this paper, the SMA wires are designed built-in pin-joints on the beam, which is different with the previous work that embedded the SMA wires in the structure [32]. Because the embedded SMA wire structure is limited by the substrate dimension, and therefore cannot provide a better contribution of SMAs in many cases. The bistable beam is firstly simplified to a single-DOF lumped model in section 2.1 without

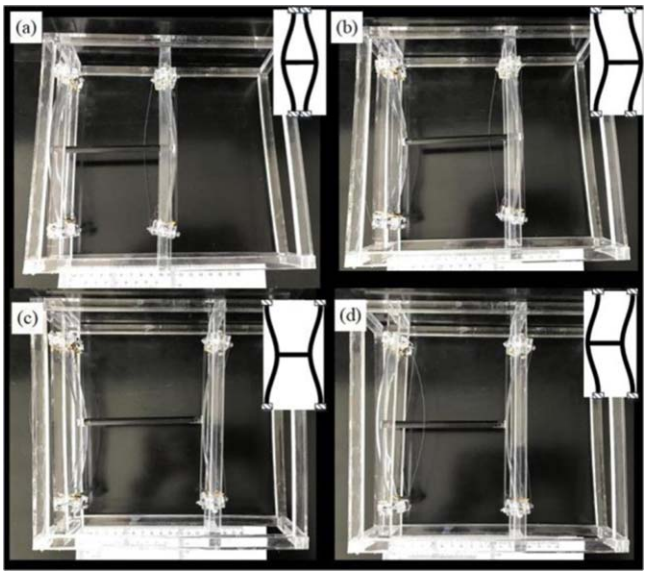

Figure 1. Top view of a laboratory-scale auxetic structure constructed by bistable beams.

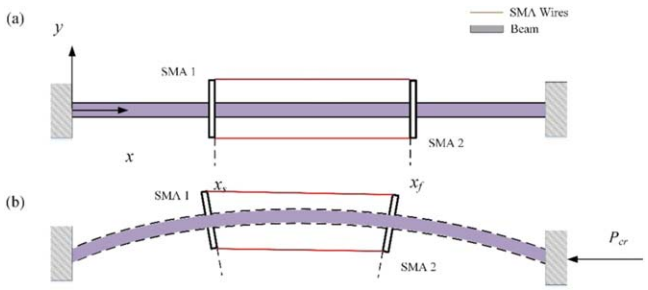

Figure 2. The shape memory alloys actuated beam model. (a) Undeformed beam. (b) Bistable beam.

considering SMA wires, and the nonlinear behaviour of bistable beams is investigated with respect to different key parameters, such as stiffness and clamp distance. In spite of its simplicity, such a mathematical model is able to capture the fundamental dynamic characteristics of a bistable beam due to its nonlinearity and instability. Then, a polynomial constitutive model of SMA is established to model the thermomechanical response for the SMA wires actuated bistable beam in section 2.2. Numerical results are obtained to analyse the switch phenomenon of SMA actuated bistable beams in section 3.1. The study of nonlinear dynamics of bistable beams was originally inspired from the investigation of an auxetic structure, as shown in figure 1. The bistable beam has the ability to snap from one stable state to the other when excited with sufficient input actuation, as such, different displacements can be achieved for this type of the auxetic structure by actuating separate bistable beams. Therefore, a bistable beam with SMA wires as the actuators is proposed as a typical bistable structural element for this auxetic system. Furthermore, section 3.2 illustrates an experimental rig that is designed for testing the stress–strain–temperature relationships of SMA in a practical SMA wires actuated bistable beam. Since the structures are considered to work under diverse situations, the

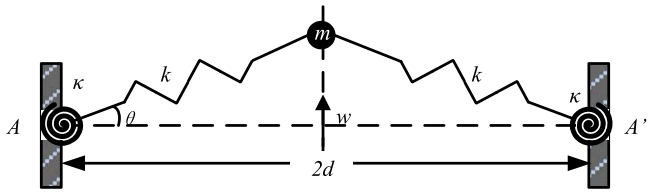

Figure 3. A simple representative buckled beam model, where a mass is supported by pairs of springs pinned to rigid supports.

nonlinear dynamic behaviour of this system under different external excitations is investigated in section 4. Numerical simulations are carried out to demonstrate the variety of responses, and compare the differences between the structural system with and without SMA wires actuating. Therefore, the topic investigated here are of interest for future research and development of SMA actuated bistable beams.

2. Spring-mass model for a continuous bucked beam

2.1. Single mass problem

A representative model for the SMAs actuated bistable beam is designed and illustrated in figure 2(a). This representative beam model is fixed at both ends, and an axial force is then applied to produce buckling, as shown in figure 2(b). Both ends of pre-stretched (5%) SMA wires are fixed with built-in pin-joints on the beam, which can be actively heated by means of Joule effects with electrical currents. Through heating the SMA wires, the bistable beam can be actively actuated to reach another stable state.

In order to establish a simplified dynamic model for the SMAs actuated bistable beams, as shown in figure 3, the beam is firstly assumed to be modelled as a discrete structure with two linear springs clamped at both ends that are used to simulate the spring stiffness and torsional stiffness at the ends [4, 39]. The mass is only allowed to move along the vertical direction with the displacement denoted by w, while the span distance of two clamped springs are $2d$. Although the springs provide the linear restoring resistance, the resulting entire system is highly nonlinear due to the geometric configuration. Therefore, this simplified system is defined by a dynamic model in the following form

$$m\ddot{w} + 2kw\left(1 - \frac{L}{\sqrt{w^2 + d^2}}\right) + \frac{\kappa\theta}{d} = 0, \tag{1}$$

where L is the original length of the springs, w is the mass displacement, k is spring stiffness, κ is torsional spring stiffness and d is the half distance between the rigid supports. θ is the inclined angle along horizontal direction

$$\theta = \tan^{-1}\frac{w}{d} \tag{2}$$

and d is defined as a linear relationship with L and a ratio α, given by

$$d = \alpha L. \tag{3}$$

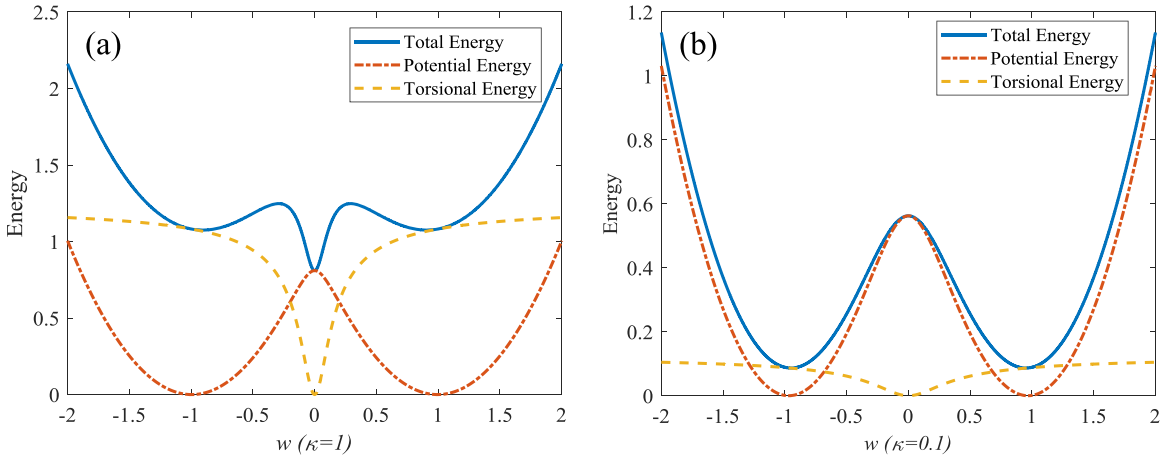

Figure 4. Effective energy E for the spring-mass model with unitary length and unitary mass ($\alpha = 0.1$). (a) $k = 1$, $\kappa = 1$. (b) $k = 1$, $\kappa = 0.1$.

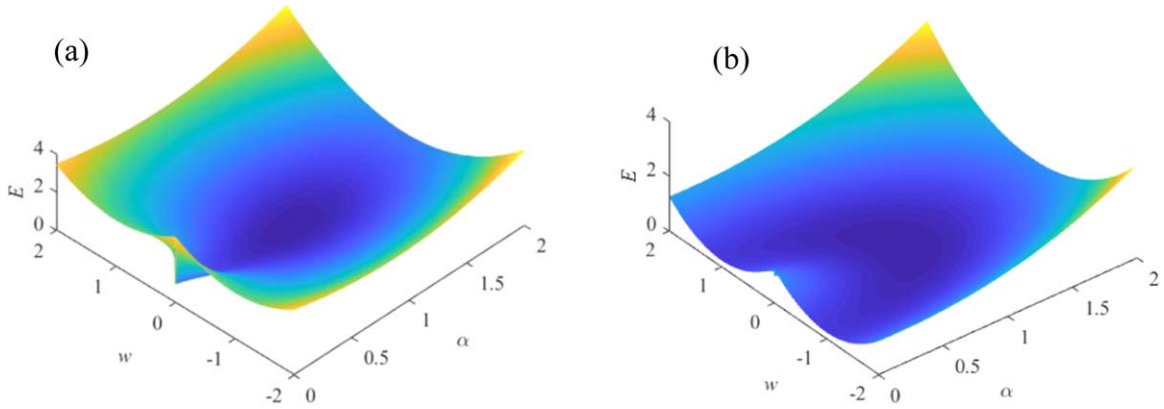

Figure 5. 3D energy plot for the spring-mass model with unitary length and unitary mass. (a) $k = 1$, $\kappa = 1$. (b) $k = 1$, $\kappa = 0.1$.

The nonlinearity in equation (1) can provide some typical dynamical behaviour in the bistable model. The nonlinear behaviour of this spring-mass system is firstly studied without considering extra forces. Therefore, the system is considered to be conservative and its effective total potential energy E is given by the sum of its potential strain energy and its torsional energy

$$\begin{aligned} E &= 2\left(\frac{1}{2}k(\sqrt{w^2+d^2}-L)^2+\int_0^{\theta}\kappa\theta d\theta\right) \\ &= 2\left(\frac{1}{2}k(\sqrt{w^2+d^2}-L)^2\right. \\ &\quad \left.+\int_0^{w}\kappa\tan^{-1}\left(\frac{w}{d}\right)\frac{d}{d^2+w^2}dw\right). \end{aligned} \tag{4}$$

The effective potential energy E of the spring-mass model with $\alpha = 0.1$ is computed and shown in figure 4, in which the different torsional spring stiffness κ results in different dynamic characteristics of the system. Figure 4(a) shows that there are three stable states (local minimum stationary points) of the spring-mass system, but a different behaviour is occurred when the torsional stiffness κ is changed, as shown in figure 4(b).

Then, in order to investigate the characteristics of the system with varying parameter α, equation (1) is rewritten as

$$m\ddot{w} = -\frac{\kappa}{d}\tan^{-1}\frac{w}{d}\left(\frac{2kd}{\kappa}\tan\frac{w}{d}\left(1-\frac{1}{\sqrt{\frac{w^2}{L^2}+\alpha^2}}\right)+1\right). \tag{5}$$

It is noted that the system may possess different multiple equilibria when $\alpha < 1$, otherwise there is only one equilibrium ($w = 0$) that exists. Clearly, if $\alpha > 1$ then the structure is in tension all the time while if $\alpha < 1$ then the structure can be both in compression and the critical buckling load can therefore to generate bistable behaviour. The 3D energy surfaces varying with respect to the mass displacement w and the ratio α are obtained using equation (3) and shown in figure 5. Although a number of equilibria of the system exists in both of figures 5(a) and (b), the system reduces its multistable characteristics dramatically when the ratio α is increasing. The corresponding bifurcation diagrams are shown in figure 6, which reveal such characteristic of the system.

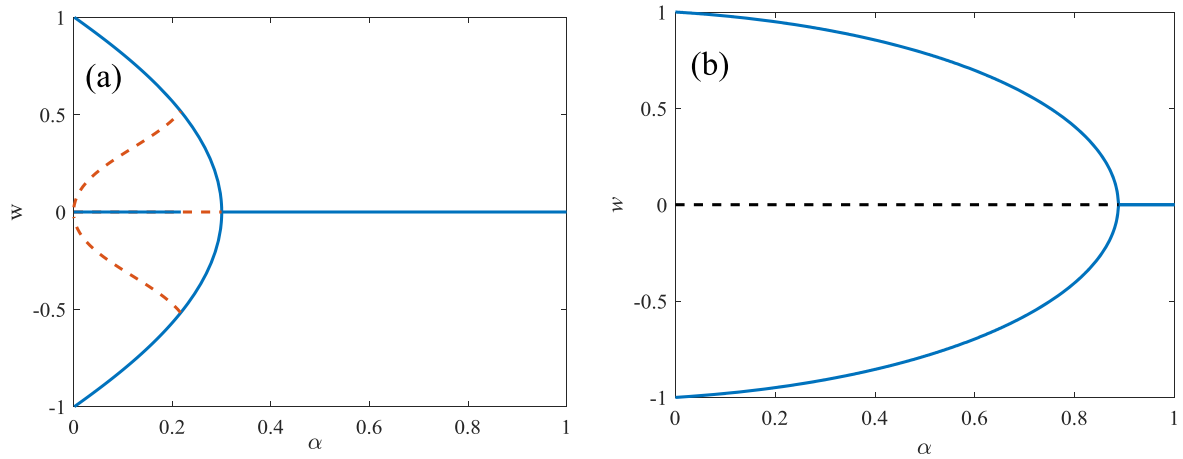

Figure 6. Bifurcation diagram for the spring-mass model with unit parameters. (a) $k = 1$, $\kappa = 1$. (b) $k = 1$, $\kappa = 0.1$.

Based on the above discussion, an updated model of a SMA wires actuated bistable beam will be developed by exploiting parts of the experimental result to determine the suitable parameters.

2.2. Updated model of a SMA wires actuated bistable beam

However, for a realistic model dissipation must also be considered, the dynamics of the problem can therefore be extended by the addition of a linear dissipation parameterised by c. Moreover, an external force induced by SMA wires is considered to construct an updated model for SMA wires actuated bistable beam, as illustrated in figure 7.

Now, the problem can be fully defined as a standard dynamical system in the following form

$$m\ddot{w} + c\dot{w} + 2kw\left(1 - \frac{L}{\sqrt{w^2 + d^2}}\right) + 2\frac{\kappa}{d}\tan^{-1}\frac{w}{d} + F_a = 0, \tag{6}$$

where c is a linear viscous dissipation coefficient, and F_a is the actuating force provided by the SMA wires to stimulate the lumped mass. The detailed geometry relationships of the SMA wires actuated bistable beam is shown in figure 7. The actuating force F_a is derived from the induced force F_s given by SMA wires

$$F_a = \frac{F_s l_{m1}}{l_{m2}} = \frac{F_s}{d}\left((l_{Ao} - d_{off}\tan\theta)\sin\theta + \frac{d_{off}}{\cos\theta}\right), \tag{7}$$

where $l_{m2} = d$, l_{Ao} is a given length between the end of the beam and the pin-joint of SMA wires. The force F_s induced by SMA wires is obtained from the SMA thermomechanical behaviour. The SMA thermomechanical behaviour is represented by a polynomial constitutive model that establishes a stress–strain–temperature ($\sigma - \gamma - T$) relation [34, 40, 41]. This constitutive model considers that the austenitic phase is stable at high temperatures, and two variants of the martensitic phase, induced by positive and negative stress fields, are

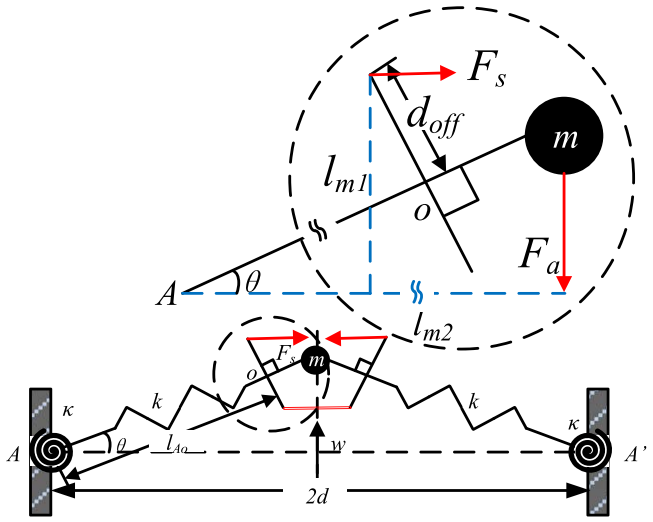

Figure 7. An updated model of a SMA wires actuated bistable beam.

stable at low temperatures

$$\sigma = a_1(T - T_M)\gamma - a_2\gamma^3 + a_3\gamma^5, \tag{8}$$

where a_1, a_2 and a_3 are material constants and T_M is the temperature below which the martensitic phase is stable. Assuming that T_A is the temperature above which the austenitic phase is stable, it is possible to write the following relationship:$a_3 = a_2^2/(4a_3(T_A - T_M))$ The force–displacement–temperature curve, therefore, is obtained using the following equation

$$F_s = A\left(a_1(T - T_M)\left(\frac{l}{l_0} - 1\right) - a_2\left(\frac{l}{l_0} - 1\right)^3 + a_3\left(\frac{l}{l_0} - 1\right)^5\right), \tag{9}$$

where A is the cross-sectional area of SMA wires and l_0 is the initial length of the pre-stretched SMA wire. Moreover, the length l of the SMA wire is varying with respect to different geometry configurations of the beam, as shown in figure 8. It

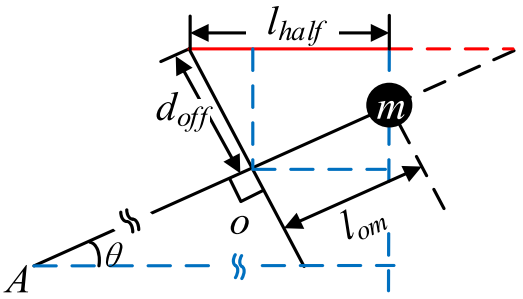

Figure 8. Actuating sketch.

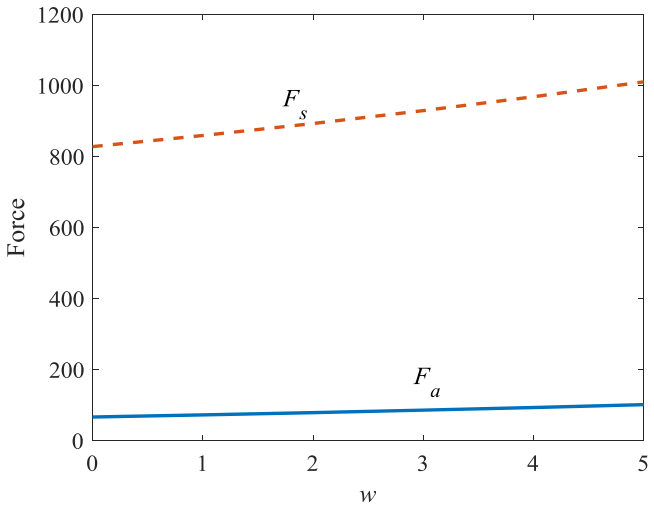

Figure 9. Force of the pre-tension (5%) SMA wire at supposed temperature 90 °C.

is finally solved by

$$l = 2l_{half} = 2(d_{off}\sin\theta + l_{om}\cos\theta), \tag{10}$$

where l_{om} is the length between joint point and mass. Therefore, equation (10) is re-expressed as

$$l = 2l_{half} = 2(d_{off}\sin\theta + (\sqrt{w^2+d^2} - l_{Ao})\cos\theta). \tag{11}$$

Although the actuation of the beam is from SMA wires, the actuating force that stimulates the beam configuration to change (buckled up and buckled down) actually is F_a. The applied force F_a on the lumped mass defined in equation (7) is finally expressed as

$$\begin{aligned} F_a = \frac{A}{d}\Bigg(& a_1(T - T_M)\Bigg(\frac{2}{l_0}(d_{off}\sin\theta \\ &+ (\sqrt{w^2+d^2} - l_{Ao})\cos\theta) - 1\Bigg) \\ &- a_2\Bigg(\frac{2}{l_0}(d_{off}\sin\theta + (\sqrt{w^2+d^2} - l_{Ao})\cos\theta) - 1\Bigg)^3 \\ &+ a_3\Bigg(\frac{2}{l_0}(d_{off}\sin\theta + (\sqrt{w^2+d^2} - l_{Ao})\cos\theta) - 1\Bigg)^5\Bigg) \\ &\times\left((l_{Ao} - d_{off}\tan\theta)\sin\theta + \frac{d_{off}}{\cos\theta}\right). \end{aligned} \tag{12}$$

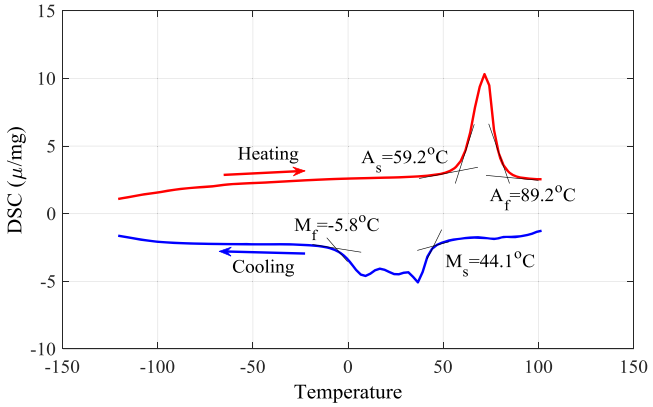

Figure 10. Measured DSC curves of SMA wires.

Table 1. Selected SMA materials properties.

Description	Value
Diameter, D (mm)	0.5
Martensite Young modulus, E_M (GPa)	22
Austenite Young modulus, E_A (GPa)	50.3
Critical stress de-twinned martensite start (MPa)	
Critical stress de-twinned martensite finish (MPa)	
Thermal expansion coefficient Θ (1×10^{-5}/°C)	1
Variation of austenite critical temperature C_A with stress (MPa/°C)	3.5
Variation of martensite critical temperature C_M with stress (MPa/°C)	10.2
Limit strain ε_L (%)	7.2

Equation (12) presents that the applied force F_a is changing along with the time-varying parameter w and the curve is plotted in figure 9. Moreover, it can be seen that the applied force F_a is approximately linear with the displacement w in figure 9, which is because of the small deflection that leads to a parametric linearization (i.e. $\sin\theta \approx \theta$).

The NiTi wires with a composition of (Ni50.1Ti49.9 at%) are used in this work and the thermo-mechanical properties of this material are listed in table 1. Moreover, the temperature variation of SMA wires during transformation is tested by differential scanning calorimeter (DSC). DSC test, which reveals the heat flow verses temperature relationship of a material upon heating and/or cooling, is one of a few standard techniques to determine the transition temperatures of materials. Figure 10 presents a typical DSC result of SMA in a heating/cooling cycle between −100 °C and 100 °C. As we can see, four different phase transition temperatures were identified using the tangent-lines method, as shown in figure 10.

Finally, by substituting equation (12) into equation (6), the fully dynamic equation of this simplified spring-mass system is obtained with the relations of $\tan\theta = w/d$ $\sin\theta = w/\sqrt{w^2+d^2}$ $\cos\theta = d/\sqrt{w^2+d^2}$, and expressed

in equation (13)

$$m\ddot{w} + c\dot{w} + 2kw\left(1 - \frac{L}{\sqrt{w^2+d^2}}\right) + \frac{A}{d}\left(a_1(T-T_M)\left(\frac{2}{l_0}\left(d_{off}\left(\frac{w}{\sqrt{w^2+d^2}}\right) + \left(\frac{\sqrt{w^2+d^2}}{2} - l_{Ao}\right)\left(\frac{d}{\sqrt{w^2+d^2}}\right)\right) - 1\right) - a_2\left(\frac{2}{l_0}\left(d_{off}\left(\frac{w}{\sqrt{w^2+d^2}}\right) + \left(\frac{\sqrt{w^2+d^2}}{2} - l_{Ao}\right)\left(\frac{d}{\sqrt{w^2+d^2}}\right)\right) - 1\right)^3 + a_3\left(\frac{2}{l_0}\left(d_{off}\left(\frac{w}{\sqrt{w^2+d^2}}\right) + \left(\frac{\sqrt{w^2+d^2}}{2} - l_{Ao}\right)\left(\frac{d}{\sqrt{w^2+d^2}}\right) - 1\right)^5\right)\left(\left(l_{Ao} - d_{off}\left(\frac{w}{d}\right)\right)\left(\frac{w}{\sqrt{w^2+d^2}}\right) + \frac{d_{off}}{(d/\sqrt{w^2+d^2})}\right) = 0. \quad (13)$$

The nonlinear dynamics of the SMA wires actuated bistable beam is now represented by equation (13), and the only parameters that need to be determined for the system are spring stiffness k and torsional spring stiffness κ. It is considered that the updated model is derived from the bistable beam, so the parameters k and κ in the updated model are obtained directly from the beam formulas [11, 42]

$$k = \frac{C_1 AE}{L}, \quad (14)$$

$$\kappa = \frac{C_2 EI}{L}, \quad (15)$$

where E is the Young's modulus, I is the moment of inertia of the cross-section, and L is the initial length of the beam. C_1 and C_2 are correction factors, and applied to the linear spring equation and the torsion spring equation, respectively. Both of them can be determined by approximating the first critical load and maximum deflection of experimental results. The full bifurcation diagram is constructed using different ratios between C_1 and C_2, as shown in figure 11.

Subsequently, a slender beam was manufactured and compressed by the testing machine as shown in figure 12, in which the two bistable configurations were observed. The initial configuration of the beam at the first stable position is illustrated in figure 12(a). The buckled beam becomes unstable after applied voltage and finally snapped into the second stable position in figure 12(b). The first critical load and maximum deflection according to the experimental result are 60 N and 2.3 mm, respectively. The parameters C_1 and C_2/C_1 are defined as 35.7 and 420 for further investigation.

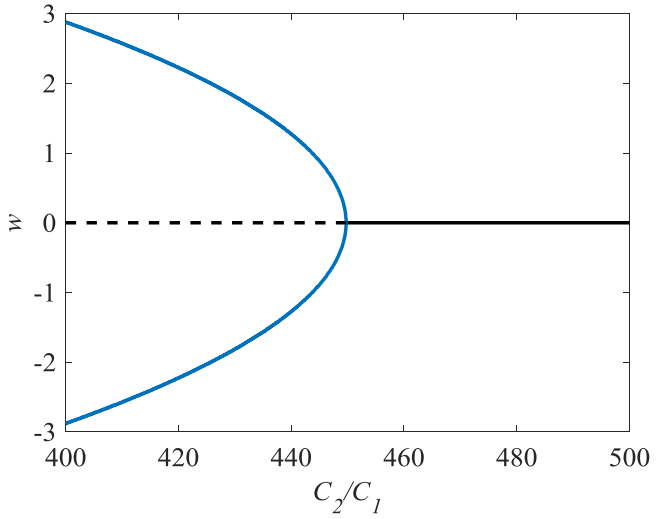

Figure 11. Bifurcation diagram for the updated model.

3. Numerical simulation and experimental validation

3.1. Numerical simulation

The governing equation for the motion of the SMA wires actuated bistable beam proposed in equation (13) is now used to study the nonlinear dynamic response of the system. The main parameters of the bistable beam are summarised in table 2.

Few further simplifications had been made in the updated model for the simulation and design of SMA wires actuated bistable beams. To calculate the central force that actuates the system, the mass of total beam was assumed to be concentrated at its geometric centre. The nonlinear dynamic response of the bistable actuated by SMA wires is determined using equation (13), and the results are plotted in figure 13. The response is affected by the system (e.g. stiffness and the actuating temperature) and the dynamic response is shown under an actuating temperature of 90 °C. The bistable switching can be achieved depending on which of the two SMA springs (as shown in figure 2) is activated. Figure 14 shows that the presence of sudden jumps in the displacement of the beam is due to the snap-through motion and one SMA wire becomes slack and the other one is suddenly under tension. For example, if the initial configuration is the one shown in figure 2(b), the SMA1 is activated to output the actuation force that drives the beam to the second stable state. When the switching process of the beam is finished, the SMA1 will become slack and SMA2 will be tensioned. During the switching process, both up (SMA1) and down (SMA2) SMA wires have nearly the same amount of strains and one is activated to stretch another one. It is obvious that

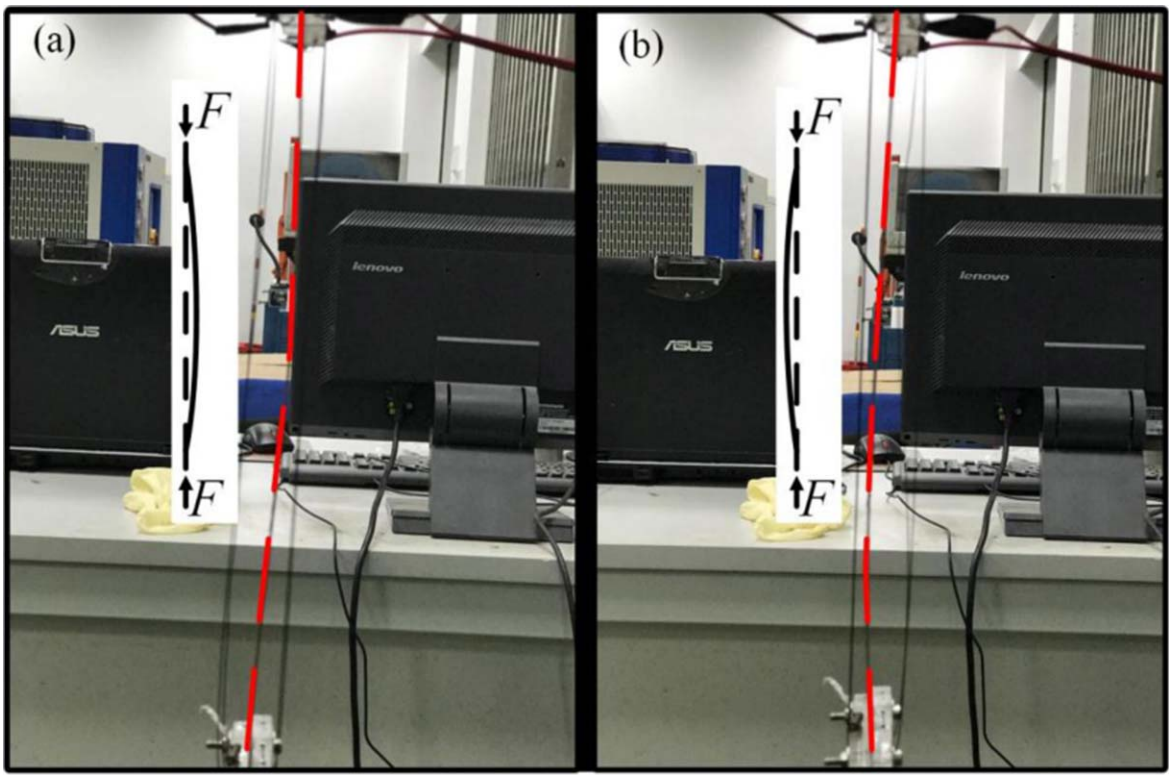

Figure 12. Photograph of the buckled beam. (a) First stable configuration. (b) Second stable configuration.

Table 2. Geometry property of the proposed beam.

Description	Value
Beam length, L, (mm)	500
Beam width, b, (mm)	30
Beam thickness, t, (mm)	1
Young modulus, E, (GPa)	206
Density, ρ, (kg mp^{-3})	8,050
Distance between supports, $2d$, (mm)	499.7
Maximum displacement, w, (mm)	2.2
SMA wire length, l_0, (mm)	250
SMA wire diameter, (mm)	0.5
Offset distance, d_{off}, (mm)	10
Distance, l_{Ao}, (mm)	125
a_1, (Pa °C^{-1})	1.28×10^9
a_2, (Pa)	2.50×10^{13}
a_3, (Pa)	5.53×10^{15}

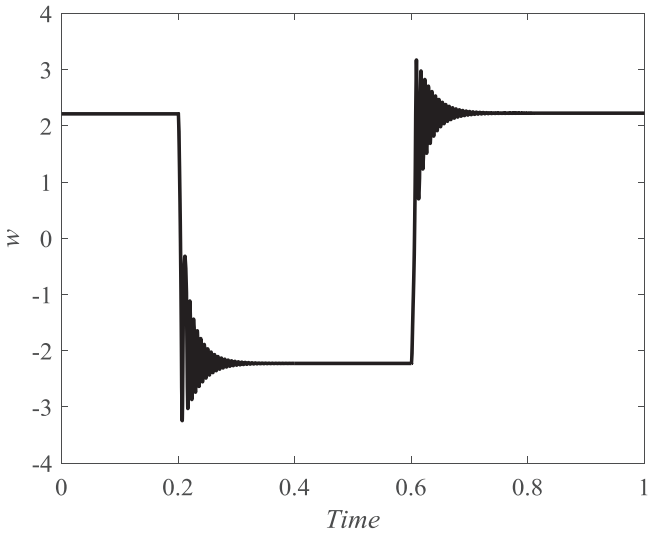

Figure 13. Simulation diagram for actuating bistable beam.

such discontinuities cannot be eliminated and may be used to design a further close loop control system.

3.2. Experimental validation

An experimental testing for the proposed SMA wires actuated bistable beam was carried out to examine the effectiveness of the updated mathematical model. The main parameters of the beam and SMA wires are the same with the simulation used in table 2. A contactless laser sensor (Keyence # LK-080) was installed side of the beam to measure the midpoint displacement w directly. Figure 14 shows that the test rig was mounted to a material test machine and the clamped force can therefore be measured directly. The edges of the beam are clamped by two holders which are also capable for translating and rotating (figure 2(a)), and the laser sensor is used to measure the middle displacement. Two separate electric circuits are connected to each side (up or down) of SMA wires and controlled by an external switch. Firstly, an initial compression (0.3 mm) is applied to produce bistable configurations (figure 2(b)). Next, one side of the SMA wires is heated

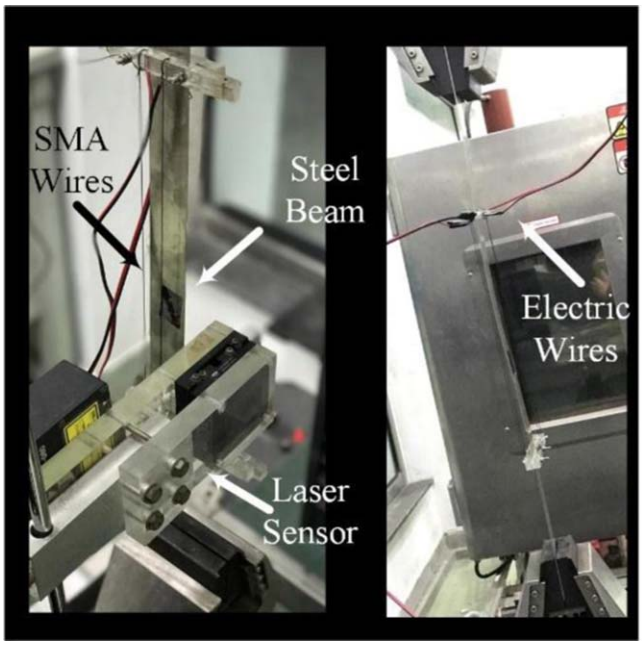

Figure 14. Photograph of the testing apparatus.

to actuate the bistable beam switch to another bistable state. The displacement of the bistable beam is measured by the laser sensor. Subsequently, a similar operation is then carried out on the other side of the SMA wires for actuating the bistable beam to recover back to its initial state. Finally, the results are processed to obtain the nonlinear dynamic response of the bistable beam.

Figure 15 illustrates the experimental results of the dynamic response of the SMA actuated bistable beam. The measured displacement of the bistable beam is plotted as a function of time and successfully demonstrated the feasibility of this design by using SMA as an actuation scheme. From this figure, it can be seen that the experimental snap through motion can be successfully stimulated through charging one of the SMA wires (SMA 1 or SMA 2) (figure 15(a)). The beam then oscillates towards the targeted stable state, and the motion gradually decays due to damping (figure 15(b)). The black solid line shown in figure 15(c) denotes the measured displacement curve for the beam, superimposed to the approximate prediction represented by the red dash line. This curve is corresponding to the first switching from convex configuration (2.2 mm) to concave configuration (−2.2 mm) indicated by the black box in figure 15(b) and the purely qualitative can be confirmed.

It is shown a good correlation between the analytical model (figure 13) and the experiments (figure 15) in terms of transition displacement of the SMA wires actuated bistable beam. The results obtained from the present mathematical model and experiment show a good agreement. This validation ensures the accuracy and applicability of the developed model. The model is therefore approved to be able to accurately predict the nonlinear dynamic characteristics of SMA wires actuated bistable beams.

4. Dynamic behaviour and chaos

Since the bistable devices can be actuated using different switching strategies: statically or dynamically, it is useful to investigate the fundamental mechanism of a bistable system influenced by the external disturbance. For example, if the external disturbance is applied at a certain frequency, the switching to the second stable state can be achieved at a lower force. Therefore, it is of vital importance to study the nonlinear dynamical behaviour of SMA wires actuated bistable beams and the contribution of activated SMAs can be provided to toggle the beam in its stable states. The proposed model is used here by rewriting the governing equation equation (6) to include an external excitation force as follows

$$m\ddot{w} + c\dot{w} + 2kw\left(1 - \frac{L}{\sqrt{w^2 + d^2}}\right) + 2\frac{\kappa}{d}\tan^{-1}\frac{w}{d} + F_a = F\cos(\Omega t), \tag{16}$$

where $F\cos(\Omega t)$ is a harmonic external force with amplitude F and frequency Ω.

The influence of actuator temperature is firstly investigated for the free vibration system ($F = 0$ N) under different cases of thermal loadings. Four cases are chosen here to provide general situations, which are system without SMA wire, temperature on 40 °C, 70 °C and 90 °C, respectively. Numerical simulation was carried out with different initial conditions to produce the corresponding nonlinear vibration responses of the system. The numerical results for the nonlinear dynamic responses of the system are presented in form of phase spaces in figure 16. Only one side of SMA wires (SMA1 or SMA 2) is considered to achieve one-way switch varying different cases. Figure 17 shows the phase space of the bistable beam with different temperatures induced SMA wires and without SMA wires, respectively.

The original system without SMA wires have three equilibria (shown as the black points in figure 16(a)), and the phase space diagram is also symmetric with respect to the vertical axis. It can be seen that two of the equilibria are stable, as same as the bifurcation diagram shown in figure 11. However, by considering the SMA wires with an initial temperature ($T = 40$ °C), the left stable equilibrium remains unchanged while the other stable equilibrium becomes smaller than before. The phase space of the system also becomes asymmetric, which means the position of the stable equilibria is changed In the other words, the shape of practical beam on two stable states will become inconsistent when one of the SMA wires is activated. Next, when the temperature is increased to ($T = 60$ °C), this characteristic becomes more obvious and it implies that the phase transformation of SMAs has been induced (from martensite to austenite). Finally, when the temperature increases to be above the austenite temperatureA_f ($T = 90$ °C), only one stable equilibrium exists. In other words, the SMA wires actuating beam will lost it original bistable feature when the stimulating temperature is larger than 90 °C.

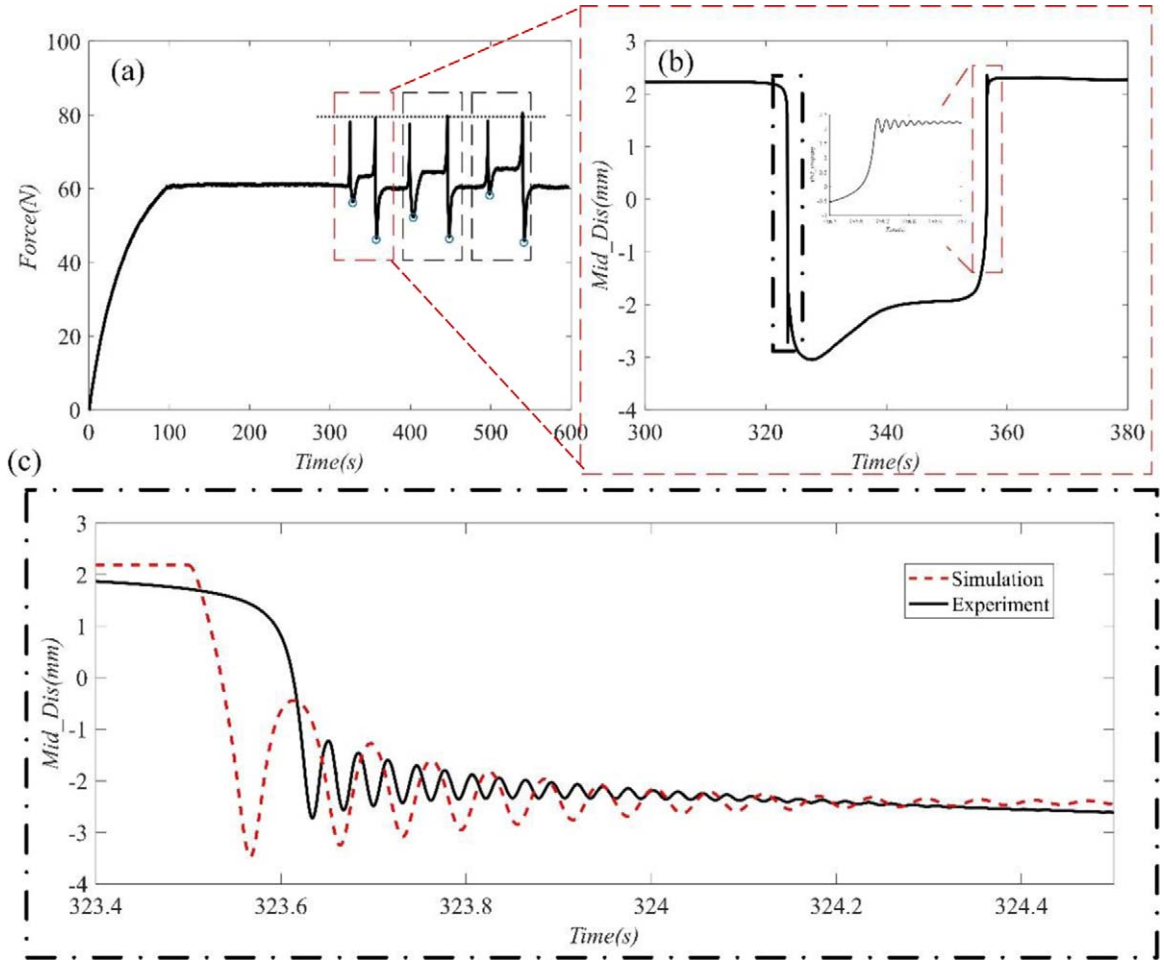

Figure 15. Experimental diagram for actuating bistable beam. (a) Force–time curve with three switching cycles. (b) Displacement–time curve in one switching process. (c) Comparison between simulation results and experimental results.

The dynamical loading is now considered in the simulation of some operational conditions for the SMA wires actuated bistable beam using equation (16). It is assumed that the bistable beam is actuated by both sides of SMA wires (SMA1 and SMA2), which means that it can be switched between two stable configurations continually. The bistable actuating configurations are of concern with an actively control with a fixed temperature ($T = 90\,^{\circ}\mathrm{C}$). Firstly, the system is studied by considering bifurcation diagrams to provide a general understanding of the system dynamics. Figure 17 presents two bifurcation diagrams showing the dynamic responses of the system when varying the amplitude F or the frequency Ω, respectively. It is noted that the change in both amplitude and frequency can cause significant different dynamic responses, for which both periodic and chaotic responses are possible. Figure 18(a) shows the dynamic responses under varying excitation amplitude F and a fixed frequency $\Omega = 100$ Hz. It can be seen that for small force amplitudes, the system emerges a periodic response until $F = 490$ N, and afterwards the system exhibits a chaotic response until another period response appears. By increasing the amplitude, the system becomes chaotic except for few periodic region, such as $F = 940$ N. On the other hand, figure 17(b) shows the system response under varying excitation frequency Ω with a fixed amplitude $F = 300$ N. It shows that, for low-frequency excitation, the system can maintain a periodic response (e.g. period-1 in $\Omega = 300$ Hz and period-2 in $\Omega = 500$ Hz). However, when the frequency reaches $\Omega = 700$ Hz, the system emerges a chaotic response.

To further study the nonlinear dynamic response of the system, it is important to analyse both the phase space and Poincare section for some special cases. Figure 18 shows the dynamic response of the bistable beam without SMA wires that are actuated under different loading conditions. Figures 18(a)–(d) present the system responses given by varying amplitude F with the fixed frequency $\Omega = 100$ Hz, which are related to the cases in figure 17(a). Figures 18(d)–(i) are the system responses given by varying frequency Ω with a fixed excitation amplitude $F = 300$ N, which are related to the cases in figure 17(b). It was found that the amplitudes of F used in all the cases are sufficiently large to produce bistable behaviour without the stimulation contribution from the SMA wires. Therefore, it is known that the cases (d)–(f) are limited by the chosen value of frequency Ω to achieve the bistable behaviour. Although different parameters may all generate chaotic responses (e.g. (b) and (h)), the characteristics of those responses are entirely different.

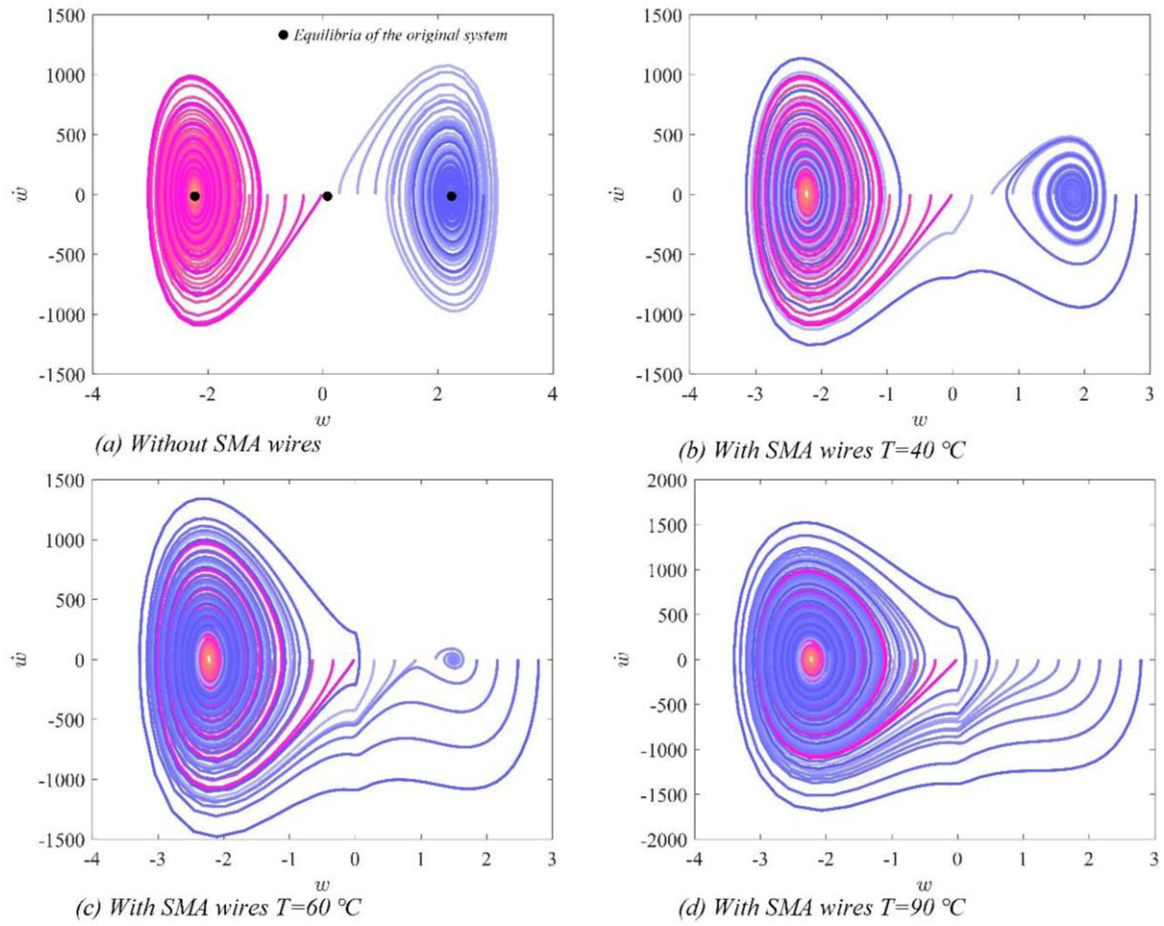

Figure 16. The bistable beam free vibration response at different temperatures. (a) Model without SMA wires. (b) $T = 40\,^{\circ}\mathrm{C}$. (c) $T = 60\,^{\circ}\mathrm{C}$. (d) $T = 90\,^{\circ}\mathrm{C}$.

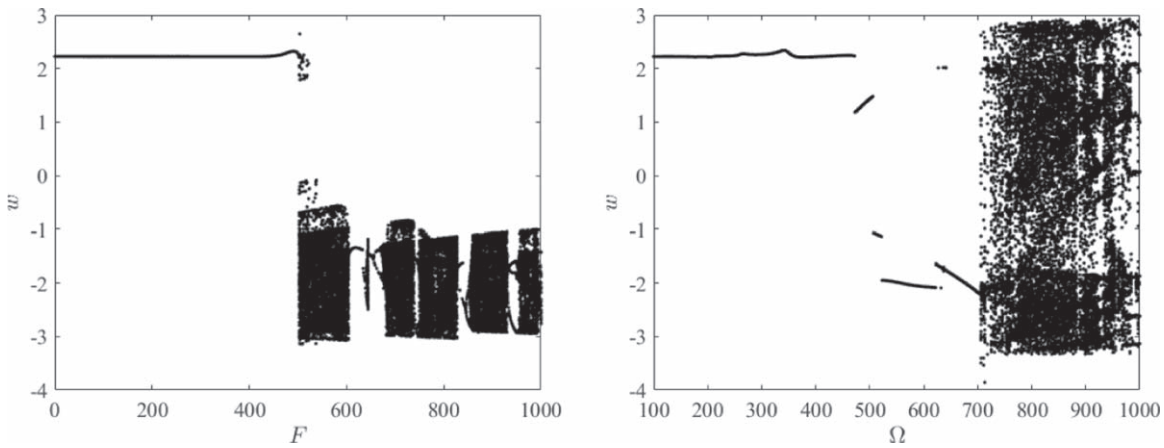

Figure 17. Bifurcation diagrams: (a) varying excitation amplitude F with a fixed frequency ($\Omega = 100$ Hz); (b) varying excitation frequency Ω with a fixed amplitude ($F = 300$ N).

Figure 19 shows the dynamic behaviour of the bistable beam with the fully activated SMA wires ($T = 90\,^{\circ}\mathrm{C}$), as once the SMA wires be activated, the property of the system will be changed. With the activated SMA wires, the system can achieve the bistable behaviour readily as shown in figure 19, which is under the same situations with figure 18. Compared with the system responses generated with or without SMA wires actuation, it was found that the influence given by the excitation force amplitude can be reduced. Figure 19(b) shows that the chaotic response can be controlled by the SMA wires, and it becomes a quasi-periodic response compared with figure 18(b). However, for different frequency excitation, the force contribution from the SMA wires is not enough to completely determine the system dynamic behaviour. It is noticeable that in the last case (i) the characteristic of the system is changed considerably, both two

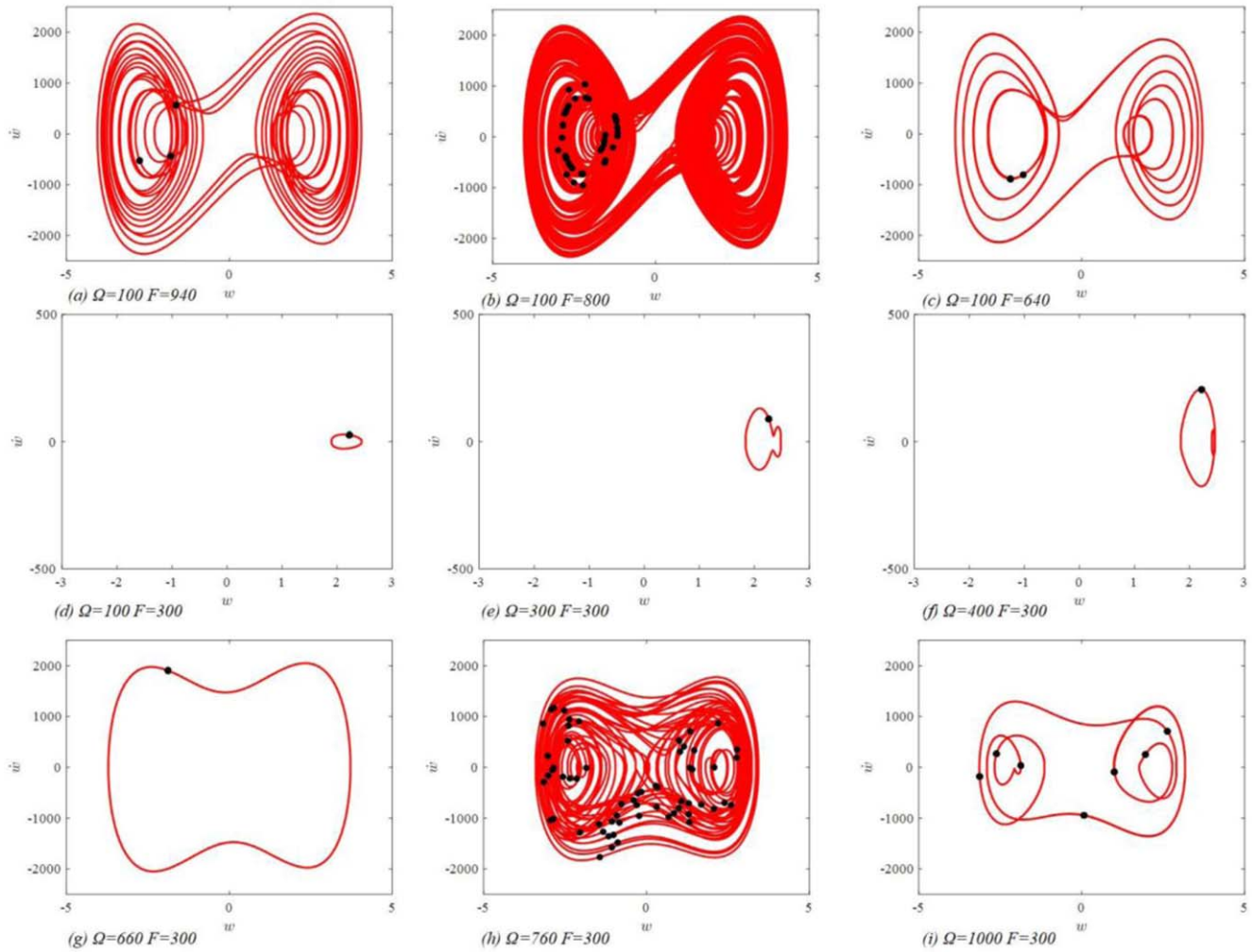

Figure 18. Response of the bistable beam without SMA wires actuating. Phase space (red lines) and Poincare section (black points). (1) $\Omega = 100$ Hz ((a) $F = 940$ N. (b) $F = 800$ N. (c) $F = 640$ N. (d) $F = 300$ N). (2) $F = 300$ N ((e) $\Omega = 300$ Hz. (f) $\Omega = 400$ Hz. (g) $\Omega = 660$ Hz. (h) $\Omega = 760$ Hz. (i) $\Omega = 1000$ Hz).

stable equilibria are disappeared, and the structure only can vibrate around the zero point.

5. Conclusion

In this paper, a representative spring-mass model of a SMA wires actuated bistable beam was developed, tested and successfully demonstrated that the stable configurations of the structure can be actively switched. A single-DOF lumped model is formed by springs and mass to show different characteristics of the bistable system by selecting the corresponding parameters. Moreover, the thermomechanical behaviour of the SMA wires is investigated to build a constitutive relation for actuating the structure, and an experimental validation has been done to show a good agreement with the numerical simulation. An updated model is then developed to investigate the dynamic characteristics of SMA wires actuated bistable beam. Numerical simulations are carried out to show the response under different external excitation situations. It was found that the different excitations (amplitude and frequency) can lead to diverse dynamic behaviours of the bistable system, including both periodic response and chaotic. However, the thermomechanical loadings produced by the SMA wires can benefit for adjusting these dynamic behaviours. Although the thermomechanical loadings can also produce complex responses including chaos, the possibility of using SMA wires to prevent the chaos happening is shown in some situations. The rich responses related to different excitations which may be caused by the potential external disturbances are analysed.

The developed bistable structures jointed with the SMA wires are capable to produce a larger deformation and a larger force, which is useful in many engineering applications, especially in small, lightweight mechanism and structures. The performance of the structures can be satisfactory predicted and the dynamical characteristic can be easily performed when the proposed simplified model is applied. Moreover, because of the cooperation of the structure and SMA wires, the SMA wire significantly affects the stability of the structure, which renders the possibility to suppress the instability of structures under specific external excitations. The limitations of such bistable structures for proper

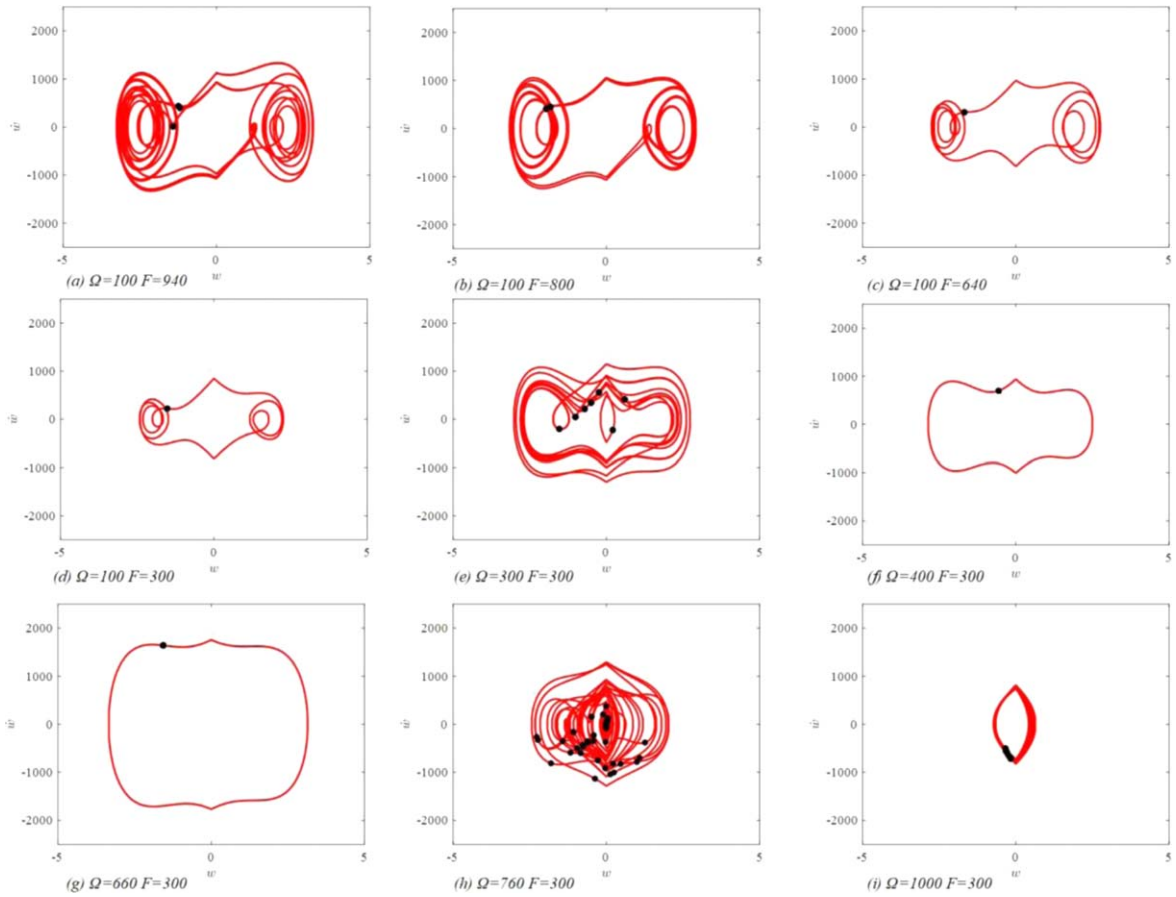

Figure 19. Response of the bistable beam with SMA wires actuating. Phase space (red lines) and Poincare section (black points). (1) $\Omega = 100$ Hz ((a) $F = 940$ N. (b) $F = 800$ N. (c) $F = 640$ N. (d) $F = 300$ N). (2) $F = 300$ N ((e) $\Omega = 300$ Hz. (f) $\Omega = 400$ Hz. (g) $\Omega = 660$ Hz. (h) $\Omega = 760$ Hz. (i) $\Omega = 1000$ Hz).

functioning can therefore be effectively broken through. The results presented in this work provide a deep understanding of physical phenomena of this type of bistable devices.

Acknowledgement

This work was supported by John Moyes Lessells Travel Scholarships of The Royal Society of Edinburgh and National Natural Science Foundation of China No.11372133.

Compliance with ethical standards

Conflicts of interest

The authors declared that they have no conflict of interest.

ORCID iDs

Jiaying Zhang https://orcid.org/0000-0001-7308-5090
Zhangming Wu https://orcid.org/0000-0001-7100-3282

References

[1] Forterre Y, Skotheim J M, Dumais J and Mahadevan L 2005 How the venus flytrap snaps *Nature* **433** 421–5
[2] Liang H and Mahadevan L 2009 The shape of a long leaf *Proc. Natl Acad. Sci. USA* **106** 22049–54
[3] Forterre Y and Dumais J 2011 Generating helices in nature *Science* **333** 1715–6
[4] McInnes C R, Gorman D G and Cartmell M P 2008 Enhanced vibrational energy harvesting using nonlinear stochastic resonance *J. Sound Vib.* **318** 655–62
[5] Zhu Y and Zu J W 2013 Enhanced buckled-beam piezoelectric energy harvesting using midpoint magnetic force *Appl. Phys. Lett.* **103** 041905
[6] Zhang J, Zhang C, Hao L, Nie R and Qiu J 2017 Exploiting the instability of smart structure for reconfiguration *Appl. Phys. Lett.* **111** 064102
[7] Zhang J and McInnes C R 2017 Using instability to reconfigure smart structures in a spring-mass model *Mech. Syst. Signal Process.* **91** 81–92
[8] Rossiter J, Stoimenov B and Mukai T 2006 A bistable artificial muscle actuator *2006 IEEE Int. Symp. on MicroNanoMechanical and Human Science* (Piscataway, NJ: IEEE) pp 1–6
[9] Pontecorvo M E, Barbarino S, Murray G J and Gandhi F S 2013 Bistable arches for morphing applications ed D Saravanos *J. Intell. Mater. Syst. Struct.* **24** 274–86
[10] Moser P, Barbarino S and Gandhi F 2014 Helicopter rotor-blade chord extension morphing using a centrifugally actuated von mises truss *J. Aircr.* **51** 1422–31

[11] Zhang J and McInnes C R 2016 Reconfiguration of a four-bar mechanism using phase space connections *Mech. Syst. Signal Process.* **81** 43–59
[12] Brinkmeyer A, Pirrera A, Santer M and Weaver P M 2013 Pseudo-bistable pre-stressed morphing composite panels *Int. J. Solids Struct.* **50** 1033–43
[13] Liu X, Lamarque F, Doré E and Pouille P 2015 Multistable wireless micro-actuator based on antagonistic pre-shaped double beams *Smart Mater. Struct.* **24** 075028
[14] Brenner M P, Lang J H, Li J, Qiu J and Slocum A H 2003 Optimal design of a bistable switch *Proc. Natl Acad. Sci. USA* **100** 9663–7
[15] Syta A, Litak G, Friswell M I and Adhikari S 2016 Multiple solutions and corresponding power output of a nonlinear bistable piezoelectric energy harvester *Eur. Phys. J.* B **89** 99
[16] Avramov K V and Mikhlin Y V 2006 Snap-through truss as an absorber of forced oscillations *J. Sound Vib.* **290** 705–22
[17] Barbarino S, Pontecorvo M E and Gandhi F 2013 Energy dissipation of a Bi-stable von-Mises truss under impulsive excitation *54th AIAA/ASME/ASCE/AHS/ASC Structures, Structural Dynamics, and Materials Conf.* (Reston, Virginia: American Institute of Aeronautics and Astronautics) (https://doi.org/10.2514/6.2013-1794)
[18] Sulfridge M, Saif T, Miller N and Meinhart M 2004 Nonlinear dynamic study of a bistable MEMS: model and experiment *J. Microelectromech. Syst.* **13** 725–31
[19] Krylov S, Ilic B R and Lulinsky S 2011 Bistability of curved microbeams actuated by fringing electrostatic fields *Nonlinear Dyn.* **66** 403–26
[20] Aimmanee S and Tichakorn K 2018 Piezoelectrically induced snap-through buckling in a buckled beam bonded with a segmented actuator *J. Intell. Mater. Syst. Struct.* **29** 1826–74
[21] Casals-Terré J, Fargas-Marques A and Shkel A M 2008 Snap-action bistable micromechanisms actuated by nonlinear resonance *J. Microelectromechanical Syst.* **17** 1082–93
[22] Flatau A B and Chong K P 2002 Dynamic smart material and structural systems *Eng. Struct.* **24** 261–70
[23] Lagoudas D C 2008 *Shape Memory Alloys: Modeling and Engineering Applications* (New York: Springer)
[24] Shu S G, Lagoudas D C, Hughes D and Wen J T 1997 Modeling of a flexible beam actuated by shape memory alloy wires *Smart Mater. Struct.* **6** 265–77
[25] Yang K and Gu C L 2008 Modelling, simulation and experiments of novel planar bending embedded SMA actuators *Mechatronics* **18** 323–9
[26] Yan Q, Wang L, Liu B, Yang J and Zhang S 2012 A novel implementation of a flexible robotic fin actuated by shape memory alloy *J. Bionic Eng.* **9** 156–65
[27] Jin H, Dong E, Xu M, Liu C, Alici G and Jie Y 2016 Soft and smart modular structures actuated by shape memory alloy (SMA) wires as tentacles of soft robots *Smart Mater. Struct.* **25** 085026
[28] Mohd Jani J, Leary M, Subic A and Gibson M A 2014 A review of shape memory alloy research, applications and opportunities *Mater. Des.* **56** 1078–113
[29] Barbarino S, Saavedra Flores E I, Ajaj R M, Dayyani I and Friswell M I 2014 A review on shape memory alloys with applications to morphing aircraft *Smart Mater. Struct.* **23** 063001
[30] Hartl D J, Lagoudas D C, Calkins F T and Mabe J H 2010 Use of a Ni60Ti shape memory alloy for active jet engine chevron application: I. Thermomechanical characterization *Smart Mater. Struct.* **19** 015020
[31] Hartl D J, Mooney J T, Lagoudas D C, Calkins F T and Mabe J H 2010 Use of a Ni60Ti shape memory alloy for active jet engine chevron application: II. Experimentally validated numerical analysis *Smart Mater. Struct.* **19** 015021
[32] Du Y, Liu B, Xu M, Dong E, Zhang S and Yang J 2015 Dynamic characteristics of planar bending actuator embedded with shape memory alloy *Mechatronics* **25** 18–26
[33] Costa D D A and Savi M A 2017 Nonlinear dynamics of an SMA-pendulum system *Nonlinear Dyn.* **87** 1617–27
[34] Rodrigues G V., Fonseca L M, Savi M A and Paiva A 2017 Nonlinear dynamics of an adaptive origami-stent system *Int. J. Mech. Sci.* **133** 303–18
[35] Barbarino S, Gandhi F S and Visdeloup R 2013 A bi-stable von-Mises truss for morphing applications actuated using shape memory alloys *Proceedings of the ASME 2013 Conference on Smart Materials, Adaptive Structures and Intelligent Systems 1* (ASME) p V001T01A004
[36] Wang W, Chan T M and Shao H 2015 Seismic performance of beam-column joints with SMA tendons strengthened by steel angles *J. Constr. Steel Res.* **109** 61–71
[37] Alves M T S, Steffen V, Castro dos Santos M, Savi M A, Enemark S and Santos I F 2018 Vibration control of a flexible rotor suspended by shape memory alloy wires *J. Intell. Mater. Syst. Struct.* **29** 2309–23
[38] Sofla A Y N, Elzey D M and Wadley H N G 2009 Shape morphing hinged truss structures *Smart Mater. Struct.* **18** 065012
[39] Zhang J and McInnes C R C R 2015 Reconfiguring smart structures using approximate heteroclinic connections *Smart Mater. Struct.* **24** 105034
[40] Falk F 1980 Model free energy, mechanics, and thermodynamics of shape memory alloys *Acta Metall.* **28** 1773–80
[41] Tanaka K, Kobayashi S and Sato Y 1986 Thermomechanics of transformation pseudoelasticity and shape memory effect in alloys *Int. J. Plast.* **2** 59–72
[42] Vogtmann D E, Gupta S K and Bergbreiter S 2013 Characterization and modeling of elastomeric joints in miniature compliant mechanisms *J. Mech. Robot.* **5** 041017